Submitted To: 1988 IEEE International Conference on Robotics and Automation

Using a Cylindrical Tactile Sensor for Determining Curvature

R.S. Fearing† and T.O. Binford
Robotics Laboratory
Department of Computer Science
Stanford, CA 94305

Abstract

This paper describes determining curvatures using a cylindrical tactile sensor. The finger touches an unknown convex surface. Principal curvatures, normal force and location are determined from a 4 by 4 window of strain measurements. Sensor strains are predicted by convolving the spatial impulse response of the rubber skin with the assumed surface pressure distribution derived from a Hertz contact model. Gradient search finds the parameters of the convex second-order shape and the force that best fit the sensor data. Experiments show radius estimation within 10%, orientation within 2.5 degrees, and subtactel localization 3% of the element spacing. We derive accuracy limits due to sensor noise.

1. Introduction

Local contact information is important for dextrous manipulation with multifingered hands. Surface features useful for grasping, such as edges and corners, can be identified by their high curvatures. Curvature also provides useful information for object identification and shape description. There has been little work in determination of curvature using tactile sensors. Speeter [1987] simulates using second differences of the strain profile to determine radius of a sphere. Montana [1986] suggests finding surface curvature by rolling a sensor without slipping about a contact. Driels [1986] and Shekhar et al [1986] found line orientation on a flat array. Brock and Chiu [1985] found surface patch orientation using repeated location measurements with a force sensor. The only tactile array curvature experiment found in the literature is Gurfinkel et al [1974] who used a 3×3 tactile sensor to find curvature using second differences of deflection.

Fearing [1987a] described sub-tactel localization, recovering normal and tangential forces, and determining line orientation on a cylinder. Inverse filtering strain measurements to determine surface deflection was considered in [Fearing, 1987b], but is limited by the low-pass nature of the elastic medium. Curvature is available from surface deflection by fitting a second order surface. This paper uses a non-linear inversion of sensed strain to obtain surface shape, which is constrained to be a paraboloid.

† current address: Dept. of Electrical Engineering,
Univ. of California, Berkeley, CA 94720

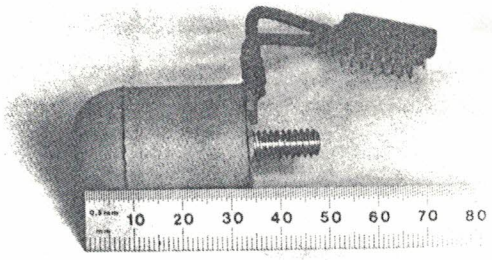

Figure 1. Tactile Sensing Finger for the Stanford/JPL Hand

2. Sensor Implementation

A tactile sensor array was packaged in a molded rubber finger tip (Fig. 1). The finger tip sensor uses an array of capacitors formed at junctions of perpendicular copper strips, spaced at 3.3 mm along the length and 18° around the circumference, of which an 8×8 subset is used. 3.8 mm of rubber covers the core and is essential to increase contact areas and reduce aliasing [Fearing and Hollerbach, 1985]. The rubber dielectric layer is a molded hollow structure (the inverse of [Siegel 1986]). Details of finger construction are in [Fearing et al, 1986 and Fearing 1987b]. Other cylindrical fingers are described by [Allen and Bajczy, 1985] and [Begej, 1986].

After calibration, the sensor output is normalized to determine equivalent strain at each tactel. The mean sensitivity of the tactels is 0.4 gram with a 3 mm diameter probe, and they are very linear up to 50 grams.

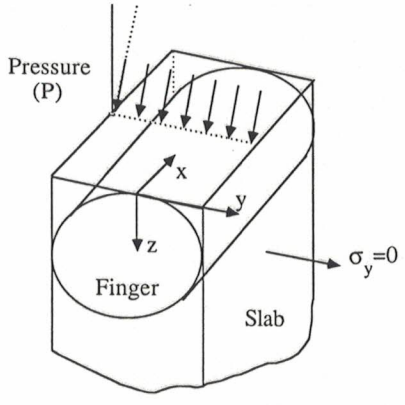

Figure 2. Coordinate System for Cylindrical Sensor

3. Impulse Response Model

We use the plane stress approximation of Fig. 2. Consider a slice of elastic material in the $x-z$ plane, with the applied force constant in the y direction, and stresses on the face $\sigma_y = 0$. For a normal line load on a linear isotropic medium, the strain is [Timoshenko and Goodier 1951]:

$$\epsilon_z(x) = \frac{-2Pd}{E\,\pi r^4}[d^2 - \nu x^2], \tag{1}$$

where P is the pressure per unit thickness of the slab in Nm^{-1}, E is the elastic modulus, ν is Poisson's ratio, d is the sensor depth, and $r^2 = d^2 + z^2$. Eq. (1) is the one dimensional *impulse response.*

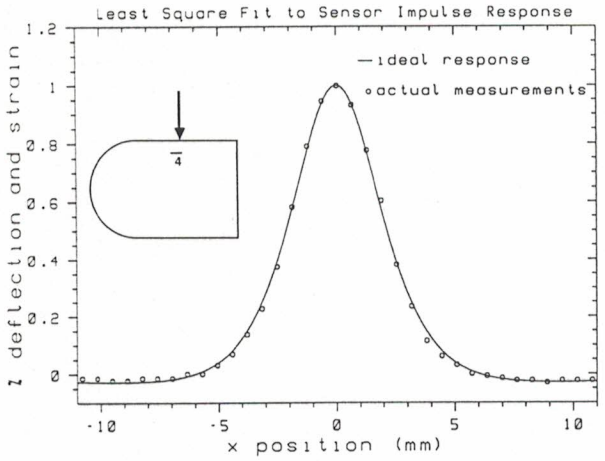

Figure 3. Plane Stress Model and Experimental Data

An approximate line load was applied normally at 0.6 mm steps along x while recording one tactel (dots in Fig. 3). Depth and Poisson's ratio parameters in (1) were adjusted to best fit the normalized samples in the least-squares sense, obtaining $d = 3.8$ mm and $\nu = 0.4$. The solid curve in Fig. 3 is the plane-stress model with these parameters, not an arbitrary best fitting curve. The root-mean-square (RMS) fitting error is 1.3% of full scale. The sensor agrees closely to the model, in spite of violating the small deflection assumption of linear elasticity.

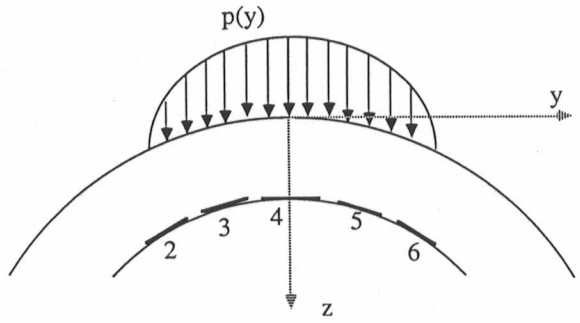

Figure 4. Sensor Geometry Around Finger Circumference

To find the two-dimensional impulse response, the cylinder is approximated by a plane (Fig. 4). The equivalent sensor spacing in the y direction is $r_f \sin\Delta\theta = 3.9$ mm, for angular spacing of 18°, where $r_f = 12.7$ mm is the finger radius. The measured response is not circularly symmetric. We do not have a theoretical model for the strain in the cylinder, thus an empirical separable impulse-response is used:

$$h(x,y) = h_x(x)\,h_y(y). \tag{2}$$

We assume a plane stress model in x and y directions,

$$h_x(x) = \frac{d_x^2\,(d_x^2 - \nu_x x^2)}{(x^2 + d_x^2)^2}, \tag{3}$$

$$h_y(y) = \frac{d_y^2\,(d_y^2 - \nu_y y^2)}{(y^2 + d_y^2)^2} \tag{4}$$

where d_x, d_y and ν_x, ν_y are equivalent depth and Poisson's ratio parameters along the cylinder axis and around the circumference. 12×11 measurements were taken with a small probe at 0.635 mm × 0.635 mm spacing along the x and y axes. Depth and Poisson's ratio parameters were adjusted to minimize mean square error between (2) and the normalized samples, obtaining $d_x = 4.3$ mm, $\nu_x = 0.5$, $d_y = 6.0$ mm, and $\nu_y = 0.7$. From [Gladwell, 1980], $\nu_y = 0.7$ with plane stress corresponds to $\nu_y^* = 0.4$ with plane strain. Fig. 5 shows deflection contours over the centralized 8×8 samples comparing normalized model and experimental data. The RMS error of the sample fit was 2.0% of full scale.

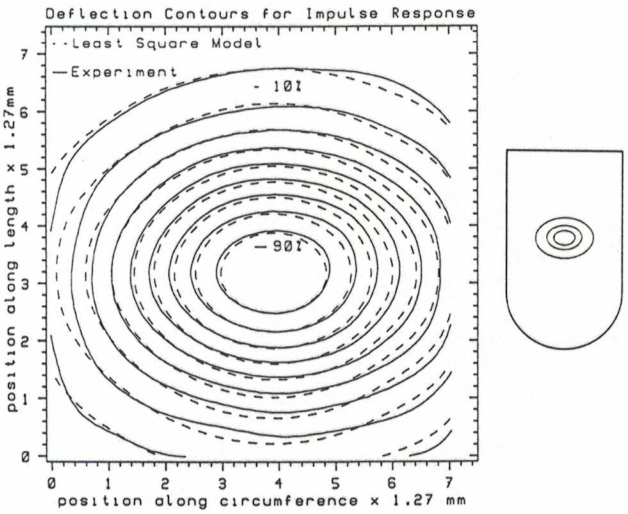

Figure 5. 2D Model and Experimental Impulse Response

4. Determining Contact Shape

We want to determine curvature of a rigid indentor pressing into a compliant finger. This section determines the shape of the contact region. Using Hertz contact approximations [Timoshenko and Goodier, 1951], (bodies are locally smooth and large with respect to deformation) the finger cylinder is approximated by:

$$z_f \approx C_f\,y^2 \tag{5}$$

where $C_f = -1/2R_f$, with R_f the finger radius (12.7 mm). (The finger axes are shown in Fig. 2). The body indenting the finger is represented by

$$z_B = A_B \tilde{x}^2 + C_B \tilde{y}^2 + \delta \tag{6}$$

where $\tilde{x}$, $\tilde{y}$ are principal curvature plane axes, δ is the indentation depth, $A_B = 1/2R_B$ and $C_B = 1/2R'_B$, with R_B and R'_B principal radii of curvature of the body.

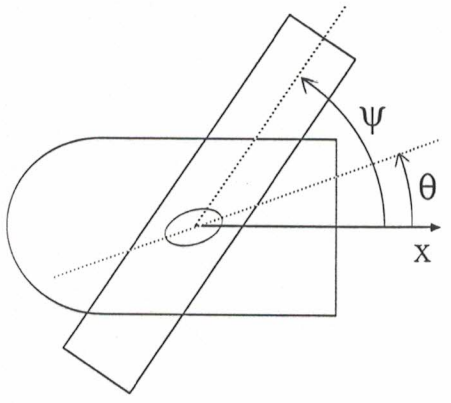

Figure 6. Cylinder Contact on Finger (Top View)

Rotating by the angle ψ from indentor to finger coordinates in (6), where ψ is defined in Fig. 6, and setting $z_f = z_B$ (the two surfaces are intersecting), we obtain

$$x^2[A_B c^2\psi + C_B s^2\psi] + 2xy\ c\psi\, s\psi[A_B - C_B]$$

$$+ y^2[C_B c^2\psi + A_B s^2\psi - C_f] = \delta\,, \tag{7}$$

where $c\psi = \cos\psi$, and $s\psi = \sin\psi$. Substituting $A = A_B c^2\psi + C_B s^2\psi$, $B = A_B - C_B$, and $C = C_B c^2\psi + A_B s^2\psi - C_f$, we see that (7) is an ellipse:

$$Ax^2 + Bxy + Cy^2 = D\ . \tag{8}$$

This contact ellipse has its major axis at the angle given by θ [Thomas, 1968] (Fig. 6) where

$$\tan(2\theta) = \frac{B}{A-C} = \frac{(A_B - C_B)\sin 2\psi}{(A_B - C_B)\cos 2\psi + C_f}\ . \tag{9}$$

For a cylindrical indentor, $A_B = 0$. (8) is rotated by θ to obtain the major and minor axes of the contact ellipse:

$$z_f = A'x'^2 + C'y'^2 \tag{10}$$

with

$$A' = Ac^2\theta + Bs\,\theta c\,\theta + Cs^2\theta$$

$$C' = As^2\theta - Bs\,\theta c\,\theta + Cc^2\theta\ .$$

As R_B increases, the orientation of the contact ellipse no longer corresponds to the orientation of the contacting cylinder.

5. Contact Pressure

The pressure distribution corresponding to a frictionless paraboloid indentation is an ellipsoid [Gladwell, 1980]:

$$p(x', y') = \frac{3F}{2\pi ab}\sqrt{1 - \frac{x'^2}{a^2} - \frac{y'^2}{b^2}}, \tag{11}$$

where a and b are the major and minor axis of the ellipsoid at $z = 0$, F is total force, and $p(x', y') = 0$ outside the contact area. Fig. 4 shows this pressure distribution in cross section. The length of the major axis of the contact ellipse [Timoshenko and Goodier, 1951] is:

$$a = m(A', C')\left\{\frac{3F(1-\nu^2)}{(A'+C')E_f}\right\}^{\frac{1}{3}} \tag{12}$$

where E_f and E_B are the elastic modulus of the finger and indenting body respectively, and it is assumed that $E_B >> E_f$. The factor $m(A', C')$ is determined from the solution of the elastic deflection equation [Gladwell, 1980] which gives the contacting ellipse size. The solution uses the complete elliptic integrals of the first and second kind, and are tabulated in [Cooper, 1969], as a function of eccentricity of the contact ellipse.

The elliptical contact can now be determined for a rigid cylinder pressed into the cylindrical finger which has $E_f \approx 2.5\times10^5\ Nm^{-2}$. For example, a 10 mm radius cylinder with its axis at 45° to the sensor, pressed with $F =$ 1N gives a contact ellipse of 11.4 mm × 3.5 mm, oriented at 26° from the x axis. Fig. 7 plots contact ellipses at 15° increments in cylinder orientation and 6 different radii for 1 N of force. A line is drawn to show scale.

Note that this representation breaks down for parallel axes, and a different formulation is needed [Gladwell, 1980]. Another limitation is that a predicted contact ellipse may be longer than the finger, because the analysis assumes an infinite length cylinder. When the contact becomes very long compared to the finger length, the surface stress will be approximately constant along any cross section orthogonal to the finger axis, and a two dimensional plane strain analysis should be valid. The contact stresses for a cylinder pressing against a plane were discussed in [Fearing and Hollerbach, 1985].

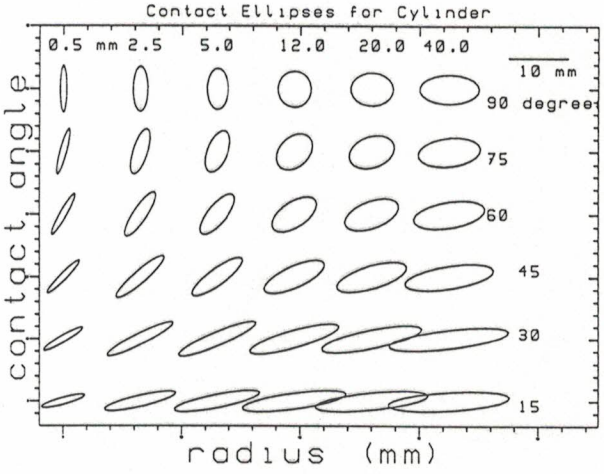

Figure 7. Contact Ellipses (to scale) for 1N

6. Curvature from Strain

Estimated sensor strain in the model is obtained from convolution of the sensor impulse response with the ellipsoidal pressure distribution of eq. (11):

$$\hat{\epsilon}_z(x,y) = h(x,y) * p(x,y) \tag{13}$$

where the planar approximation from section 3 is used. The equations are outlined as:

$$\left[\begin{array}{c} R_1, R'_1, \psi, F \\ \text{contact} \\ \text{parameters} \end{array}\right] \rightarrow \left[\begin{array}{c} a,\ b,\ \theta,\ P \\ \text{ellipsoid} \\ \text{parameters} \end{array}\right] \rightarrow \tag{14}$$

$$\left[\begin{array}{c} h(x,y) \\ \text{impulse} \\ \text{response} \end{array}\right] \rightarrow \hat{\epsilon}_z(x,y)$$

where $\hat{\epsilon}_z$ is the predicted strain. Using the a priori constraint that the contact is a paraboloid, we want to invert (14) to obtain contact parameters from measured strain values.

The tactile sensor discrete samples are represented by

$$\epsilon_z[m,n] = \epsilon_z(m\,\Delta x, n\,\Delta y) \tag{15}$$

where $\Delta x \approx 3.3$mm and $\Delta y \approx 3.9$ mm are the sensor spacing. The Mean Square Error (MSE) between model and experimental values is calculated for a 4×4 region of the array that contains the peak strain value:

$$MSE = \xi^2 = \frac{1}{4\times4}\frac{1}{\max \epsilon_z} \sum_n \sum_m (\hat{\epsilon}_z[n,m] - \epsilon_z[n,m])^2. \tag{16}$$

This expression is normalized by the maximum strain measured on the sensor, so $\sqrt{MSE}$ corresponds to the standard deviation of each element's fit to the model as a percentage of the peak strain.

The MSE is minimized by a gradient search technique, where the set of parameters for a cylinder including the center position of the contact x_o, y_o is:

$$\overline{\alpha} = [R_1\ F\ \psi\ x_o\ y_o]^T . \tag{17}$$

The search is started from the interpolated center of pressure, which corresponds to the peak strain location [Fearing et al 1986]. The interpolation error due to aliasing is ±0.4 mm along x and ±0.5 mm along y. The gradient adjustment of position eliminates this position error.

The main point is to recover curvature from the cylindrical tactile sensor, not to extract it in the most computationally optimal manner, so slow convergence of the gradient method is not a major issue. The error surface was examined for several cases, and found to be bowl shaped locally, so techniques such as Newton's Method could give faster convergence. In experiments, the gradient search converges to the global minimum, albeit slowly in some trials.

7. Sensitivity to Error

We examine cylinder radius and orientation estimation limits due to sensor noise. Impulse response modelling errors and limitations from the planarity and frictionless indentation assumptions are neglected. We define 2 error vectors:

$$\Delta\underline{R} = \left(\Delta R_1, \Delta\psi, \Delta F\right)^T , \tag{18}$$

the parameter estimation error, and the sensor error

$$\Delta\underline{\epsilon}_z = \left(\Delta\epsilon_{z\,11}, \Delta\epsilon_{z\,22}, \cdots, \Delta\epsilon_{z\,43}, \Delta\epsilon_{z\,44}\right)^T . \tag{19}$$

We want to determine $\max \Delta\underline{R}$, the maximum expected error in the radius, force, and orientation estimates as a function of $\max \Delta\underline{\epsilon}_z$, the worst case strain sensor error. The measured normal strain is represented as a vector function $\underline{f}()$:

$$\underline{\epsilon}_{zo} = \underline{f}(R_o, \psi_o, F_o). \tag{20}$$

For small strain errors, $\underline{f}$ is expanded in a Taylor's series about nominal values:

$$\underline{\epsilon}_z \approx \underline{\epsilon}_{zo} + \Delta\underline{\epsilon}_z = \underline{\epsilon}_{zo} + J\,\Delta\underline{R} , \tag{21}$$

where J is the Jacobian of $\underline{f}()$. For a 4×4 array of sensors, J is a 16×3 matrix. The least-squares matrix solution [Strang, 1980] for $\Delta\underline{R}$ is:

$$\Delta\underline{R} = (J^T J)^{-1} J^T\ \Delta\underline{\epsilon}_z = A\,\Delta\underline{\epsilon}_z , \tag{22}$$

where $A = (J^T J)^{-1} J^T$. $J^T J$ is well-conditioned for the measurement range used here.

With i.i.d. noise, the covariance matrix is:

$$\Lambda_R = A\ \sigma_\epsilon^2 I\ A^T = AA^T\sigma_\epsilon^2 = \sigma_\epsilon^2 (J^T J)^{-1} \tag{23}$$

where σ_ϵ^2 is the individual sensor noise variance. We found that sensor noise with no load is due to quantization [Fearing, 1987b]. The strain signal has quantization steps of 0.1% ($\delta\epsilon_z = \pm0.05\%$), corresponding to 0.3 gram sensitivity with a 3 mm diameter probe.

Given bounds on expected sensor error ($\Delta\underline{\epsilon}_z$), the worst case expected error for each parameter is found independently. Examining the rows of A, the maximum parameter change in each element of $\Delta\underline{R}$ will occur when $\Delta\underline{\epsilon}_z$ is aligned with $\underline{A}_i$, the i th row of A. That is

$$\max\Delta R = \underline{A}_1^T \Delta\underline{\epsilon}_z = \underline{A}_1^T \frac{\underline{A}_1}{|\underline{A}_1|} |\Delta\underline{\epsilon}_z| = |\underline{A}_1||\Delta\underline{\epsilon}_z| \tag{24}$$

Similarly, $\max\Delta\psi = |\underline{A}_2||\Delta\underline{\epsilon}_z|$ and $\max\Delta F = |\underline{A}_3||\Delta\underline{\epsilon}_z|$. The length of the sensor error vector is simply

$$|\Delta\underline{\epsilon}_z| = \sqrt{\Delta\underline{\epsilon}_z{}^T \Delta\underline{\epsilon}_z} \leq \sqrt{N}\,\delta\epsilon_z \tag{25}$$

with N the number of tactels in the window. Thus $|\Delta\underline{\epsilon}_z| \leq 0.2\%$. Note that error sensitivity may not be uniform. That is, the rows of A could be $\underline{A}_i^T = [0\ 0\ 0 \cdots 1\ 0\ 0]$, with all parameter sensitivity due to error at a single tactel. However, the rubber skin spreads strain to all sensor sites, and thus in practice error sensitivity is well distributed over the central tactels in the window.

Maximum bounds on each parameter are directly related to the covariance matrix. That is, max ΔR, $\Delta\psi$, and ΔF are the diagonal elements of AA^T, the covariance matrix (23).

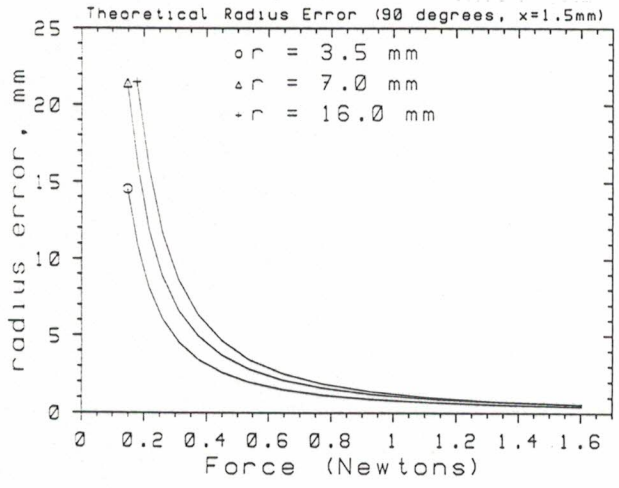

Figure 8. Force Dependence of Radius Error Sensitivity

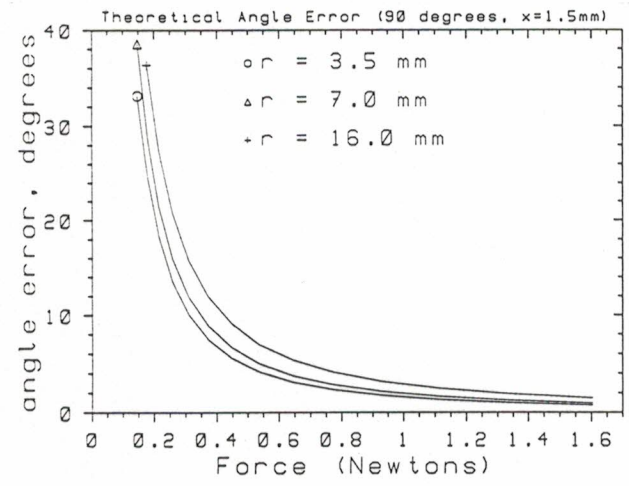

Figure 9. Force Dependence of Angle Error Sensitivity

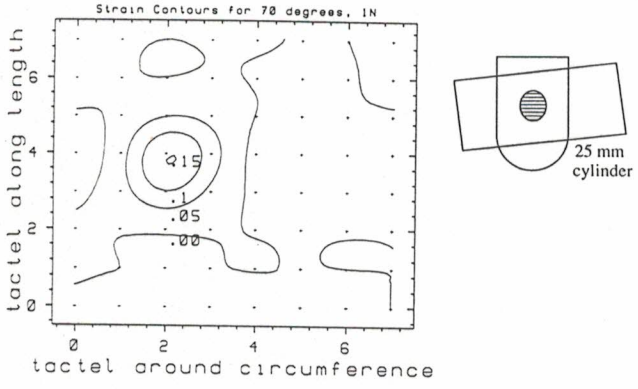

Figure 10. Strain Contours for 25 mm Cylinder at 70°

7.1. Error Dependence on Applied Force

Parameter estimation error bounds are evaluated using quantization noise. Predicted errors in radius and orientation estimation were numerically calculated as a function of force for cylinders at 90° to the finger axis, with the contact location half way between tactels (Fig. 8 and 9). Better performance is obtained with increased contact force (improved S/N ratio), and thus greater tactel output and larger contact area. Radius estimates are not usable unless the force is greater than about 50 grams. Angle error is reduced with a smaller diameter cylinder, which is expected because the contact ellipse becomes more eccentric, making orientation less ambiguous.

The bound on force error ΔF was calculated as a function of applied force and cylinder radii (not shown). Interestingly, force error is relatively independent of force, radius, or angle of the contacting cylinder, and is $< \pm 1.5$ gram. Error bounds as a function of indenting cylinder orientation in the range 30° to 150°, were determined for 1 Newton force. In the central region (axes perpendicular), we expect less than 10% error in radius for a 12.5 mm radius cylinder. Errors increase as the cylinder and finger axis get closer to alignment. Localization error $\Delta x \leq 0.03$ mm for a 14 mm diameter cylinder pressed against the finger at 90°. This position error is just 1% of the tactel spacing along the finger length.

8. Experimental Results

Curvature estimation was tested by pressing a cylindrical probe normally into the finger, and measuring the 8×8 tactel array. The strains were linearized by a look-up table. The residual sensor strain (hysteresis) was zeroed before each measurement. A Delrin or aluminum probe is attached to a balance beam, and the applied force is controlled to 5% by the weight on the beam. The finger is mounted on a machinist's table and is positioned under the stationary probe. The table is accurate to 25 μm in translation, and about 0.1° in rotation.

The low pass property of the skin complicates extracting angle and radius information from strain. Fig. 10 shows contours of constant strain for a 25 mm diameter cylinder applied at 70° with 1 N force. It is apparent from this pattern that heuristic methods of curvature or direction estimation are not likely to be very successful.

The 4 impulse response parameters (d_z, d_y, ν_z, ν_y), the modulus of elasticity, and the sensor spacing (determined from design parameters 3.3 mm and 18°) are not adjusted by the gradient search.

8.1. Cylinder Diameter

Cylinders were applied orthogonally to the finger above tactel [2 4] to eliminate cell variation effects. Sect. 8.3 shows that force and radius estimation are position independent. Fig. 11 plots sensed versus actual cylinder diameter (details in Table 1). Radius errors are < 1 mm, which agrees with the error bound of Fig. 8, except for the 66 mm diameter cylinder. The 66 mm cylinder contact ellipse is 9.9×5.5 mm, which may be too large for the planar assumption. Force is estimated to about 10% except for larger diameters, but the error analysis predicts $\Delta F < 0.015N$. Gain variations from calibration may cause this error. If estimates are close to the "maximum" error then systematic error in the sensor model has more effect than quantization.

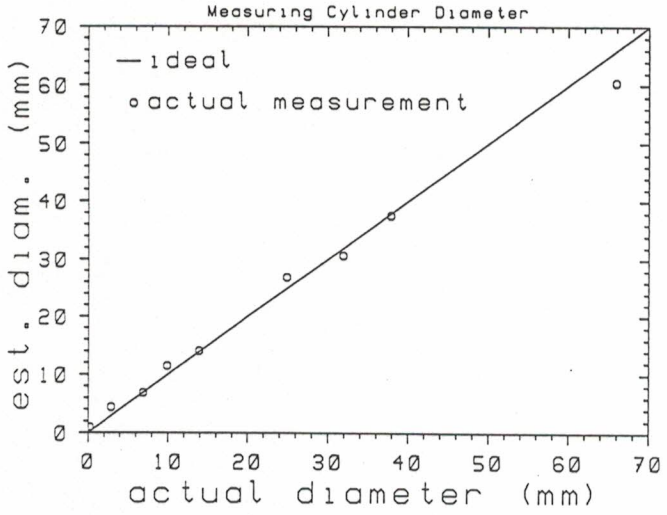

Figure 11. Estimated Cylinder Diam. for $\psi = 90°$

Table 1. Determining Cylinder Diameter for Contact at 90°

Diam.	Force (N)	Est. Diam.	Est. Force	$\sqrt{MSE}$
0.3	0.5	1.1	0.42	3.09%
3	0.5	4.5	0.49	2.78%
7	1.0	7.0	0.96	2.15%
10	1.0	11.6	1.09	2.95%
14	1.0	14.2	0.91	1.56%
25	1.0	27.0	1.02	1.78%
32	1.0	30.8	1.07	1.69%
38	1.0	37.7	1.19	2.11%
66	1.0	60.6	1.16	2.16%

The RMS error ($= \sqrt{MSE}$) in Table 1 suggests how well gradient search fit a paraboloid indentor to measured strain. RMS error of $< 3\%$ of full scale is good compared to the 2% RMS fitting error for the impulse response of Sect. 3, and here there are additional error sources. Better fit (lower RMS error) seems to be correlated with better radius estimation.

The estimated ellipsoid width $a = 2.25$ mm for the 10 mm diameter cylinder contact is smaller than the 3.3 mm sensor spacing. This sub-tactel "resolution" is possible because the surface deflection is a second-order function, and thus the space of possible strain functions is constrained.

8.2. Cylinder Orientation

Good angle estimation was obtained with a 25 mm diameter cylinder (Fig. 12). The cylinder was applied with 1N force at a random position, not above element [2 4]. The random position did not reduce accuracy; angle error $\Delta\psi$ ($\pm 3°$ near $90°$) is within predicted bounds of Fig. 10. Radius estimates are unreliable as the cylinder axis gets close to the finger axis. Here the predicted contact ellipse extends beyond finger cylinder ends, but is still aligned with the tactile samples.

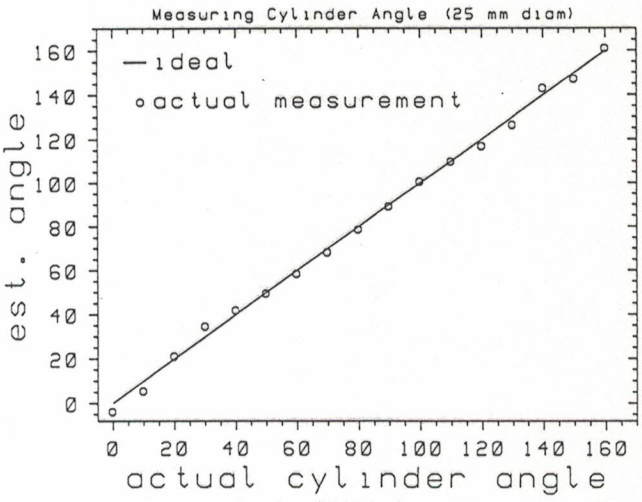

Figure 12. Sensed Orientation for 25 mm Diam. Cylinder

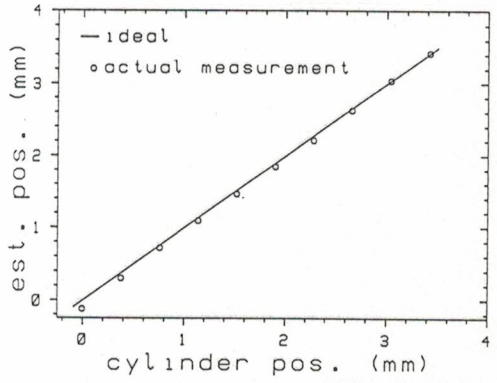

Figure 13. Tracking Cylinder Position

8.3. Position Independence

A 14 mm diameter cylinder perpendicular to the finger was moved along the x axis in 0.381 mm steps. The gradient search (eq. 16) here includes position, and the plot of sensed and ideal location is shown in Fig. 13. Residual errors are $<\pm 0.1$ mm, or just 3% of the tactel spacing. Since the sensor is hand fabricated, the sensor spacing may be 3.2 mm instead of the ideal value. Note that the cylinder indents into the finger about 0.4 mm, which is a significant position change when compared to the localization.

The radius estimate for this experiment seems to have random fluctuations ($< \pm 0.5$mm) as a function of position. The force estimate has little variation ($< \pm 0.05$ N) and is consistently low, which may be due to a balance beam or model error. Contact location dependencies were not seen.

8.4. Determining Both Principal Curvatures

The previous sections used the cylinder-contact constraint. We now find both curvatures, R_1 and R_1'. Since there is one more parameter to find, we might expect noisier estimates, because our measurement set is statistically less adequate. Note that the ellipsoid space (two axes, one orientation, one amplitude) has enough dimensions to be unique for every curvature and force combination. The contact ellipse may be the same for different surfaces, but the amplitude of the ellipsoid will distinguish between them.

Experiments with three spheres are summarized in Table 2. The contact ellipse is aligned with the x and y axes, as expected. The curvature error was greater in the circumference direction (R'), as expected due to the lower frequency response along y. R' for the large sphere was estimated rather poorly. Radius error bounds for the 28.5 mm radius sphere in the y direction, $\Delta R'$, was found to be 8 times the radius error ΔR in the x direction. With a 1 N load, ΔR is about 1.5 mm, which explains some of the R' error. Another error source is the Hertz contact assumptions when contacts are large compared to finger size. The cylinder constraint is not necessary for proper convergence; as seen in Table 2 for a 25 mm cylinder, we found R within 25% and $R' >> R$.

Edges and vertices are interesting features which provide secure grasping points and can be characterized by a very small radius of curvature in at least one direction, (see Table 2). For a plane we sensed two large contact radii, but the contact is parallel to the finger axis, and therefore suspect. This is the same as a large cylinder aligned with the finger.

Table 2. Determining Both Principal Curvatures.

Object	R	R'	Est. R	Est. R'	$\sqrt{MSE}$
sphere	1.5	1.5	1.1	0.1	2.03%
sphere	18.5	18.5	20.3	22.2	1.77%
sphere	28.5	28.5	25.7	52.8	3.30%
knife	0.2	$>>1$	0.5	41.0	3.30%
cyl. edge	≈ 0	12.5	0.6	22.0	4.65%
cylinder	12.5	$>>1$	15.5	200.3	1.67%
plane	$>>1$	$>>1$	150.0	11.7	5.18%
vertex	≈ 0	≈ 0	0.0	0.0	5.08%

9. Summary and Future Work

Experimental results show accurate angle determination to $\pm 3^\circ$, for cylinders. Radius estimation is fairly good, $\pm$2mm or so when the cylinder is at right angles to the finger. Force sensing is the least accurate, although 10% is usable. It would not be easy to servo on the force estimates because of elastic hysteresis, and the computational complexity.

The experimental conditions tend to give a best case performance. The cylindrical probe was aligned horizontally and normally to be directly above the finger. The forces were large enough to be outside the quantization level, but small enough to be close to the sensor linear range. The probes were smooth, thus the frictionless indentation assumption is reasonable.

There are many modelling errors. Gain calibration is only accurate to 5%. Copper strip positioning during fabrication causes sensor position errors. The measured "strains" are really large scale deflections, not infinitesimal quantities. The separable impulse response model is wrong, and can cause problems for contacts that are not along one axis.

The sensor sensitivity and density is adequate for estimating cylinder diameters and orientation, and diameters of small spheres. The algorithm should be expanded to handle cylinders in alignment with the finger axis, and any case where the contact goes to the end of the finger. A new rubber material would reduce hysteresis and increase stability. When the curvature sensing runs in real time, it will be quite useful for high-level tactile feedback with the Stanford/JPL hand.

Acknowledgements

This work was supported by DARPA contract MDA903-86-K-0002. Many thanks to G. Gorali for his excellent work on finger design and construction, and to B. Armstrong, S. Shekhar and D. Kriegman for helpful dialogue.

References

P. Allen and R. Bajczy, "Object Recognition using Vision and Touch," 9th Int. Joint Conf. on Artif. Intell., Los Angeles, Aug. 1985.

Begej Corporation, "Model FTS-2 Fingertip-shaped Tactile Sensor," Technical Bulletin #2, Oct. 1986.

D. Brock and S. Chiu, "Environment Perception of an Articulated Robot Hand Using Contact Sensors," ASME Winter Annual Meeting, Miami, FL, 1985.

D.H. Cooper, "Hertzian Contact-Stress Deformation Coefficients", *Jnl. of Applied Mech.*, vol. 36, no. 2, June 1969.

M.R. Driels, "Pose Estimation using Tactile Sensor Data for Assembly Operations," IEEE Int. Conf. on Robotics and Auto., San Francisco, CA April, 1986.

R.S. Fearing and J.M. Hollerbach, "Basic Solid Mechanics for Tactile Sensing," *Int. Jnl. of Robotics Research*, vol. 4, no. 3, Fall 1985.

R.S. Fearing, A. Rise, and T.O. Binford, "A Tactile Sensing Finger Tip for a Dextrous Hand," SPIE Conf. on Intell. Robotics and Computer Vision, Cambridge, MA Oct. 1986.

R.S. Fearing, "Some Experiments with Tactile Sensing during Grasping," IEEE Int. Conf. on Robotics and Auto., Raleigh, NC April, 1987a.

R.S. Fearing, "Tactile Sensing, Perception, and Shape Interpretation", Ph.D. Thesis, Dept. of Elect. Eng., Stanford Univ., Dec. 1987b.

G.M.L. Gladwell, *Contact Problems in the Classical Theory of Elasticity*, Netherlands: Sijthoff and Nordhoff, 1980.

V.S. Gurfinkel, A. Yu. Shneyder, Ye. M. Kanayev, and Ye. V. Gurfinkel, "Tactile Sensitizing of Manipulators", *Engineering Cybernetics*, vol. 12, no. 6, Nov. 1974.

D.J. Montana, "Tactile Sensing and the Kinematics of Contact", Ph.D. Thesis, Div. of Appl. Sci., Harvard Univ., August 1986.

S. Shekhar, O. Khatib, M. Shimojo, "Sensor Fusion and Object Localization," IEEE Int. Conf. on Robotics and Auto., San Francisco, CA April, 1986.

D.M. Siegel, "Contact Sensors for Dextrous Robotic Hands," MIT AI Lab Technical Report 900, June 1986.

T.H. Speeter, "Analysis and Control of Robotic Manipulation", Ph.D. Thesis, Dept. of Biomed. Eng., Case Western Reserve Univ., Jan. 1987.

G. Strang, *Linear Algebra and its Applications*, San Diego: Harcourt Brace Jovanovich, 1980.

G.B. Thomas, *Calculus and Analytic Geometry* Reading, MA: Addison-Wesley 1968.

S. Timoshenko and J.N. Goodier, *Theory of Elasticity*, New York: McGraw-Hill, 1951.